

# Hammer-Shaped Element-Based Compact MIMO Antenna for WLAN Application

Vinay Sharma<sup>\*</sup>, Madhur D. Upadhayay, Atul V. Singh, and Jitendra Prajapati

**Abstract**—This paper proposes a dual-polarized and high gain, four-element based compact multiple-input-multiple-output (MIMO) antenna operating at 5.2 GHz. First, a hammer-shaped antenna has been designed with a gain of 5.3 dBi, impedance bandwidth of 400 MHz, and broadside radiation. A mathematical analysis for radiated electric field and an equivalent circuit model of the hammer-shaped antenna are developed. Using the hammer-shaped antenna as an element, four element MIMO design with shorting walls is proposed. The shorting walls near non-radiating edges improve isolation between the elements by changing the direction of the major lobe. The proposed MIMO design has an envelope correlation coefficient (ECC)  $< 0.15$ , measured gain of 5.5 dBi, and mean effective gain (MEG)  $\sim -3$  dB. This design has a low profile and single layer planar structure of area  $65 \text{ mm} \times 65 \text{ mm}$ , which makes it a good contender for portable devices or low-profile hand-held applications in WLAN band.

## 1. INTRODUCTION

MIMO systems are the key facilitator for wireless technologies like WiMAX, WLAN (Wireless Local Area Network), and LTE (Long Term Evolution). These systems employ multiple antenna elements for improving system parameters like capacity and coverage, while overcoming problems of multipath fading [1, 2]. As the next generation compact devices have limited space, multiple antennas have to be placed in close proximity. Due to this adjacency, (electromagnetic) mutual coupling among antenna elements arises which degrades the system performance [3]. Several literatures have examined the problems related to improving capacity as well as reducing mutual coupling in a MIMO system [4–15]. The widely used capacity enhancement method in MIMO antenna is spatial diversity, which includes angle and pattern diversities. In this approach, antenna elements are placed orthogonally to attain spatially shifted radiation patterns [4–7].

To mitigate the effects of mutual coupling in MIMO antennas, Defected Ground Structures (DGS) and planar parasitic elements are used commonly [5–14]. Another method to reduce mutual coupling is the use of ground coupled resonating loops loaded with lumped elements to tune the resonance [10]. In a few studies sometimes along with the lumped elements, diodes have also been used to improve isolation and reconfigure the properties of antenna elements [11]. Impedance bandwidth is one of the most important parameters of any antenna structure. One commonly used method to enhance the impedance bandwidth is to place the antenna on a cavity made of electrical walls [4]. Also, characteristic mode theory can be used to generate adjacent modes for bandwidth enhancement. These modes are generated by selecting optimum feed point locations on a given geometry to resonate in a specific mode [15]. Orthogonal polarization improves the diversity gain of MIMO antenna. Orthogonal polarization can be attained using orthogonally arranged self-complementary structures [5]. Also, to achieve angle and polarization diversity, two concentric rings excited with four ports can be used, where two ports are positioned orthogonally. The replication of designs with DGS and CSRR requires cost intensive techniques, and DGS may behave as an unwanted parasitic radiator [6].

---

*Received 16 March 2021, Accepted 13 April 2021, Scheduled 19 April 2021*

<sup>\*</sup> Corresponding author: Vinay Sharma (vs816@snu.edu.in).

The authors are with the Department of Electrical Engineering, Shiv Nadar University, Uttar Pradesh, India.

In a few studies, monopole antennas have also been investigated for MIMO applications [7–9]. Neutralization lines have been used to improve isolation among monopoles [7]. A single layer simplistic design [8] using monopoles has been realized to emulate MIMO capability. The ground connected to monopoles behaves as a radiator, where the ground size affects radiation characteristics. These antennas have provided a large bandwidth with a very low gain [7–9].

In this paper, first a hammer-shaped antenna (gain of 5.3 dBi) is analysed, then a four-port dual polarized miniature MIMO antenna is proposed for 5.2 GHz WLAN band applications. The proposed MIMO design has a very low profile (65 mm × 65 mm) and high gain (5.5 dBi), which make it suitable for hand-held device applications. This MIMO antenna design also provides pattern diversity which improves its overall performance.

## 2. ANTENNA ELEMENT DESIGN

The hammer-shaped antenna is realized by two back-to-back connected rectangular patch antennas. These rectangular patches are made with length ( $l$ ) = 13 mm and width ( $w$ ) = 12.5 mm. The back-to-back connection is made through a microstrip line of length =  $a$  (6 mm) and width =  $b$  (2 mm). To design the hammer-shaped antenna, an FR4 substrate of size 50 mm × 40 mm × 1.6 mm ( $h$ ) has been used with substrate permittivity ( $\epsilon_r$ ) = 4.1. The antenna is excited with a microstrip line (50  $\Omega$ ) and uses a quarter wave transformer for the impedance matching. The schematic diagram of the antenna design is shown in Fig. 1(a) and simulated using CST Microwave Studio.

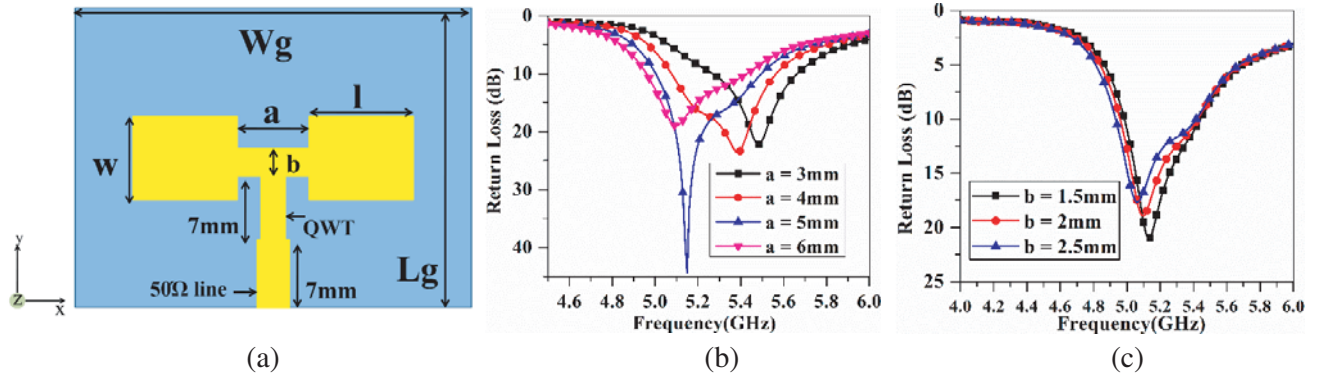


**Figure 1.** (a) Hammer shaped antenna. (b) Simulated results for variation in ‘ $a$ ’ from 3 to 6 mm at  $b = 2$  mm. (c) Simulated results for variation in ‘ $b$ ’ from 1.5 to 2.5 mm for  $a = 3$  mm.

A parametric study is performed to optimize the hammer-shaped antenna. For the optimization study, parameters ‘ $a$ ’ and ‘ $b$ ’ are varied as shown in Figs. 1(b) and 1(c) keeping all other parameters constant. As observed from the figures, increasing the value of length  $a$ , the resonance frequency shifts to a lower frequency band; increasing length ‘ $b$ ’ the resonance frequency shifts to a lower frequency band, and impedance matching degrades. For 5.2 GHz WLAN band application, the optimum values of  $a$  and  $b$  are found to be 6 mm and 2 mm, respectively.

An equivalent circuit model for the hammer-shaped design has been developed using the transmission line model of microstrip antenna and is shown in Fig. 2(a). The antenna is modelled using a parallel RC circuit, equivalent to slot impedances [16]. The T networks is modelled as a combination of series inductors and shunt capacitors. The optimized values of equivalent parameters are:  $L_1 = 0.095$  nH,  $L_2 = 4.03$  nH,  $L_3 = 3.6925$  nH,  $C_1 = 0.246$  pF,  $C_2 = 0.06922$  pF,  $C_3 = 0.5$  pF,  $R_1 = 0.85$  Ohm. A comparison of simulated (full wave field solver) measured, and equivalent circuit model return losses is shown in Fig. 1(b). It can be observed that the antenna resonates at 5.2 GHz, and simulated, equivalent circuit model, and measured results are in good agreement. The simulated and measured return loss values are 20 dB and 27 dB, respectively, with impedance bandwidths of 456 MHz and 410 MHz, respectively.

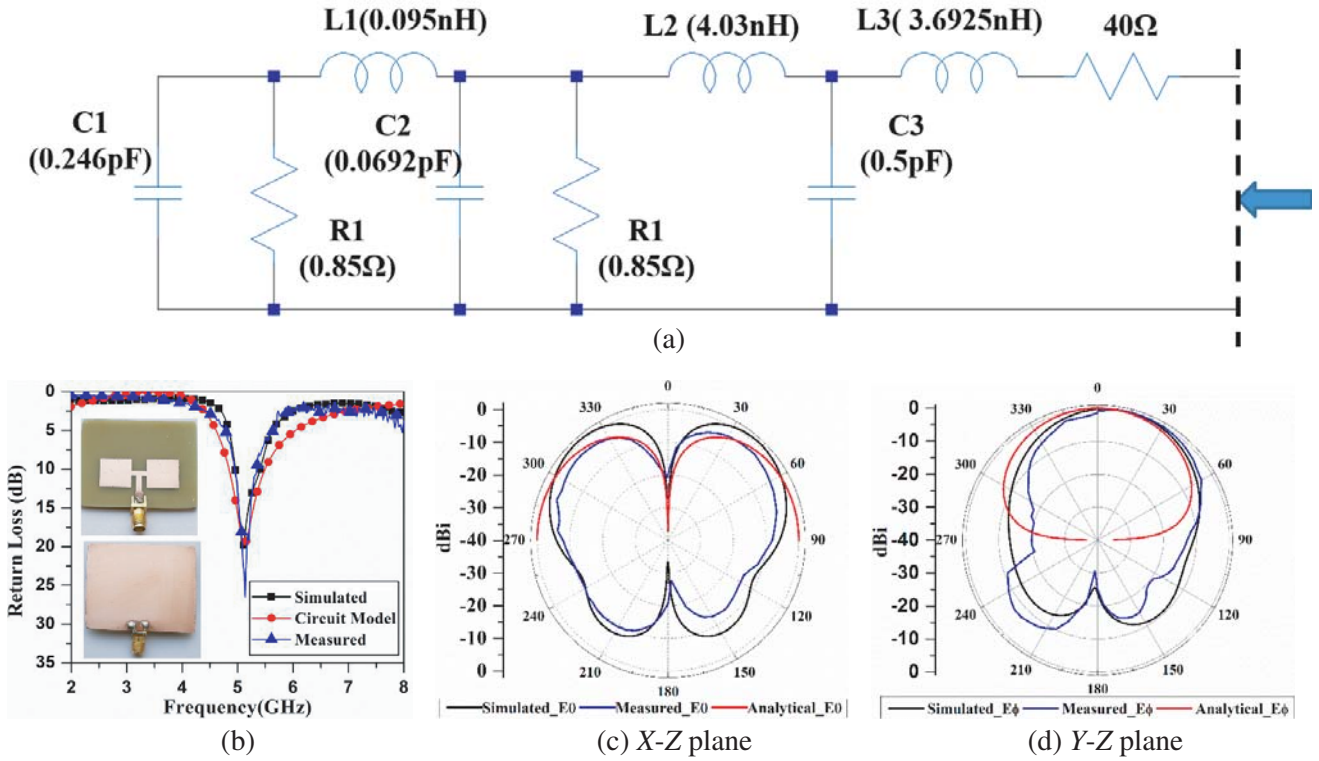


**Figure 2.** (a) Equivalent circuit model of hammer shaped antenna. (b) Comparison between simulated, measured and equivalent circuit model return loss of hammer shaped antenna. (c) Simulated, measured and analytical radiation pattern (normalized) for hammer shaped element at 5.2 GHz in X-Z plane. (d) Simulated, measured and analytical radiation pattern (normalized) for hammer shaped element at 5.2 GHz in Y-Z plane.

In order to analyze an antenna, different types of analytical methods have been reported in the literature [17, 18]. An effort has been made to develop a mathematical analysis of the hammer-shaped antenna. The analysis is based on the cavity model [16], and the radiated electric field components ( $E_\theta$  and  $E_\phi$ ) of the hammer-shaped antenna can be written as:

$$E_\theta = E_{\theta_{\max}} \left( e^{j0.3k_x} - e^{-j0.3k_x} \right) \cos \left( \frac{lk_x}{2} \right) \tag{1}$$

$$E_\phi = E_{\phi_{\max}} \left( e^{j0.3k_x} - e^{-j0.3k_x} \right) \cos \left( \frac{lk_x}{2} \right) \tag{2}$$

where,  $k_x = \beta \sin \theta \cos \phi$ ,  $k_y = \beta \sin \theta \sin \phi$ ,  $K_z = \beta \cos \theta$ ,  $k = \sqrt{k_x^2 + k_y^2 + k_z^2}$ ,  $\beta =$  phase constant,  $E_{\theta_{\max}} = w \times h \times E \times \cos \phi \times \frac{jke^{-jkr}}{4\pi r}$ ,  $E_{\phi_{\max}} = -w \times h \times E \times \sin \phi \cos \theta \times \frac{jke^{-jkr}}{4\pi r}$

$$E = \left( \frac{\sin(0.5hk_z)}{0.5hk_z} \right) \left( \frac{\sin(0.5whk_y)}{0.5whk_y} \right)$$

The obtained radiation pattern results from the analytical modelling are compared with the simulated and measured results at 5.2 GHz as shown in Fig. 2. It can be seen from Fig. 2(c) that X-Z plane has two major lobes directed along 45° which have beamwidths of 50° each. In Y-Z plane (Fig. 2(d)), only one major lobe is present with a beamwidth of 60°. The slight variation in the analytical results occurs due to the basic assumptions of the cavity model [16]. The hammer shape antenna has a high gain (simulated = 5.9 dBi, measured = 5.3 dBi) and broadside radiation pattern. The hammer shape antenna element has higher gain and directivity than a basic patch antenna at 5.2 GHz [16].

### 3. MIMO ANTENNA DESIGN

This section deals with MIMO antenna design using four hammer-shaped elements placed orthogonally. All the elements are excited separately to realize a four-port MIMO antenna with dual polarizations. The proposed MIMO antenna has a size of  $65\text{ mm}(L) \times 65\text{ mm}(L) \times 1.6\text{ mm}$ . Four elements are placed orthogonally where the edge-to-edge distance between the neighbouring elements is  $d = 14\text{ mm}$ , and the distance between element edge and substrate edge is  $e = 2\text{ mm}$ .

In order to maintain the isolation between the ports, four shorting walls are placed at  $6\text{ mm}$  away from the non-radiating edge of each antenna element as shown in Fig. 3(a). The surface area of each shorting wall is  $32\text{ mm} \times 2\text{ mm}$ . Isolation between the ports (co-polarized Port 1 and Port 3) for different values of  $L$  with and without shorting wall is shown in Fig. 3(b). It can be seen that the reduction in the antenna size ( $L \times L$ ) degrades the isolation between the ports. However, the introduction of shorting walls improves the isolation, impedance matching, as well as reduction in the overall size of proposed MIMO antenna as shown in Fig. 3(b) and Fig. 3(c), respectively. It can be observed from the MIMO antenna radiation patterns shown in Figs. 3(d) and 3(e). Due to the change in major lobe direction, the mutual coupling among ports decreases, and the isolation between the ports of the same polarization improves. This introduction of the shorting wall reduces the intensity of side lobes, thus directing all power towards the major lobe.

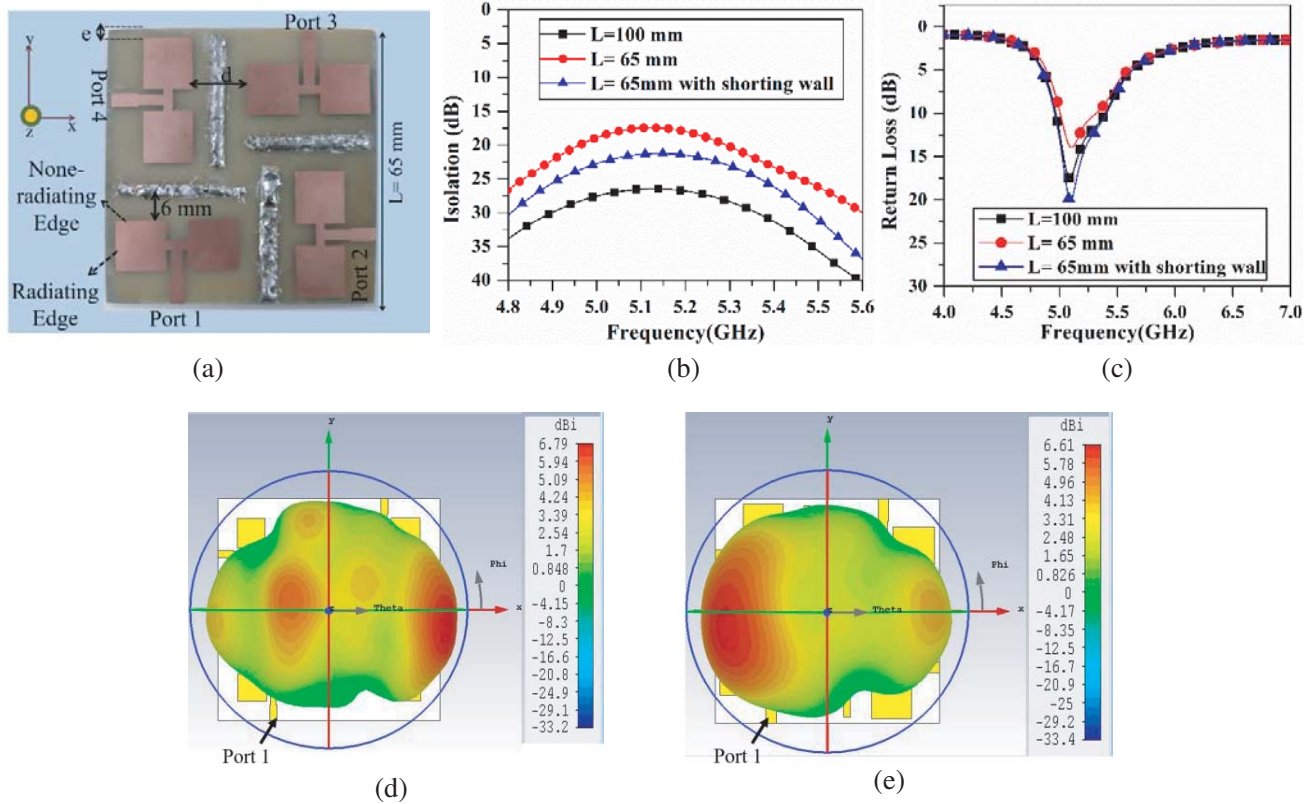


**Figure 3.** (a) Fabricated Prototype of proposed MIMO design. (b) Comparison of isolation between the elements (Port 1 and Port 3). (c) Comparison of simulated return loss with and without shorting wall (Port 1). (d) Radiation pattern of proposed MIMO design ( $L = 65\text{ mm}$ ) with excitation provided at port 1 without shorting wall. (e) Radiation pattern of proposed MIMO design ( $L = 65\text{ mm}$ ) with excitation provided at port 1 with shorting wall.

To verify the design, a comparison of simulated and measured results of the return loss and isolation in the proposed MIMO design are shown in Fig. 4. The proposed MIMO design covers the range from  $4.95\text{ GHz}$  to  $5.35\text{ GHz}$  with an impedance bandwidth of  $400\text{ MHz}$  and good isolation higher than  $22\text{ dB}$ .

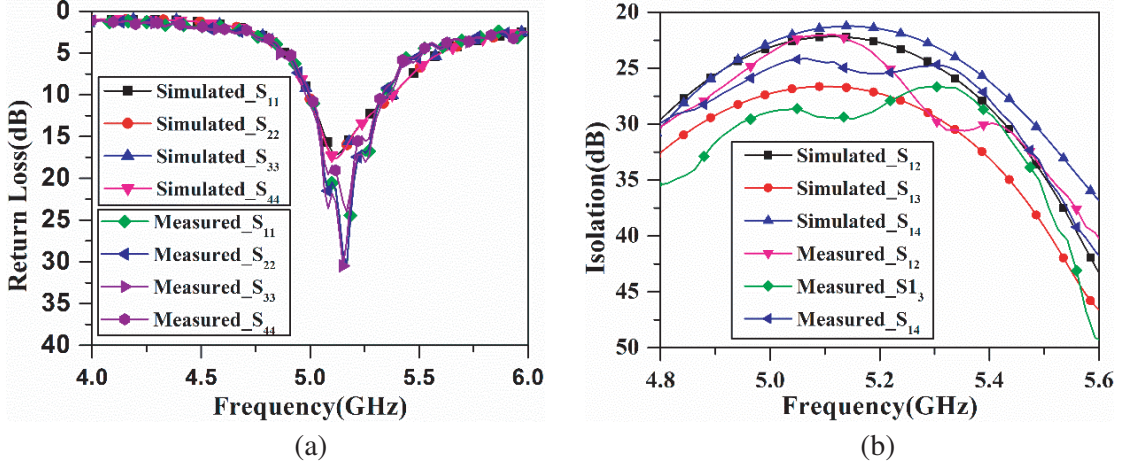


**Figure 4.** Simulated and measured  $s$ -parameters for proposed MIMO design. (a) Return loss. (b) Isolation when excitation provided to port 1.

The 2D normalized radiation patterns (of proposed MIMO design) at 5.2 GHz in  $X$ - $Z$  and  $Y$ - $Z$  planes are shown in Fig. 5(a), Fig. 5(b), Fig. 5(c), Fig. 5(d). The radiation patterns are measured using a vector network analyser (NI-PXIe-1078) with a standard horn antenna as a reference and our proposed MIMO antenna as a test antenna. These radiation patterns are obtained by exciting one port at a time while keeping other ports terminated with matched load, which makes them behave as passive radiators.

The major lobe directions corresponding to excitation of Port 1 and Port 2 are along the negative  $X$ -axis and negative  $Y$ -axis, respectively. As Port 3 and Port 4 are mirror images of Port 1 and Port 2, respectively, the corresponding radiation patterns can be found by taking mirror image of respective radiation patterns. Considering  $X$ -axis directed radiation patterns as Horizontal Polarization (HP) and  $Y$ -axis directed patterns as Vertical Polarization (VP), the proposed MIMO design has two orthogonal polarization states, which improves the mutual coupling between orthogonal elements. The simulated and measured gain profiles of the antenna are shown in Fig. 5(e). The gain profile is almost constant over the band of operation; however, the peak gain value is 6 dBi (sim.) and 5.5 dBi (meas.) at 5.1 GHz.

#### 4. MIMO PERFORMANCE ANALYSIS

The maximum channel capacity of the proposed MIMO design is calculated using the following Equation (3) from [11] with measured signal power in Line of Sight (LOS) scenario assuming cross-polarization discrimination (XPD) value of 0 dB as shown in Fig. 6(a):

$$C = \log_2 \left( \det \left[ I + \frac{SNR \times HH^*}{N} \right] \right) \quad (3)$$

where  $SNR$ ,  $H$ ,  $H^*$ ,  $N$ , and  $I$  denote signal-to-noise ratio, channel matrix, conjugate channel matrix, noise power, and identity matrix, respectively. It is observed that the capacity of the MIMO antenna increases with the  $SNR$  value in comparison to the single antenna element.

Mutual coupling among antenna elements degrades the spectral efficiency in the MIMO system, and ECC (Envelop correlation coefficient) quantifies these effects. Equation (4) is used to calculate ECC [19]. The comparison of measured and simulated ECC values for the MIMO antenna are shown in Fig. 6(b). It is observed that the ECC values meet the industry-standard ( $< 0.3$ ) [8].

$$ECC_{ij} = \frac{\left| \oint E_{\theta i}(\Omega) \cdot E_{\theta j}^*(\Omega) + E_{\phi i}(\Omega) \cdot E_{\phi j}^*(\Omega) \right|^2}{\left( \oint E_{\theta i} \cdot E_{\theta i}^* + E_{\phi i} \cdot E_{\phi i}^* d\Omega \right) \times \left( \oint E_{\theta j} \cdot E_{\theta j}^* + E_{\phi j} \cdot E_{\phi j}^* d\Omega \right)} \quad (4)$$

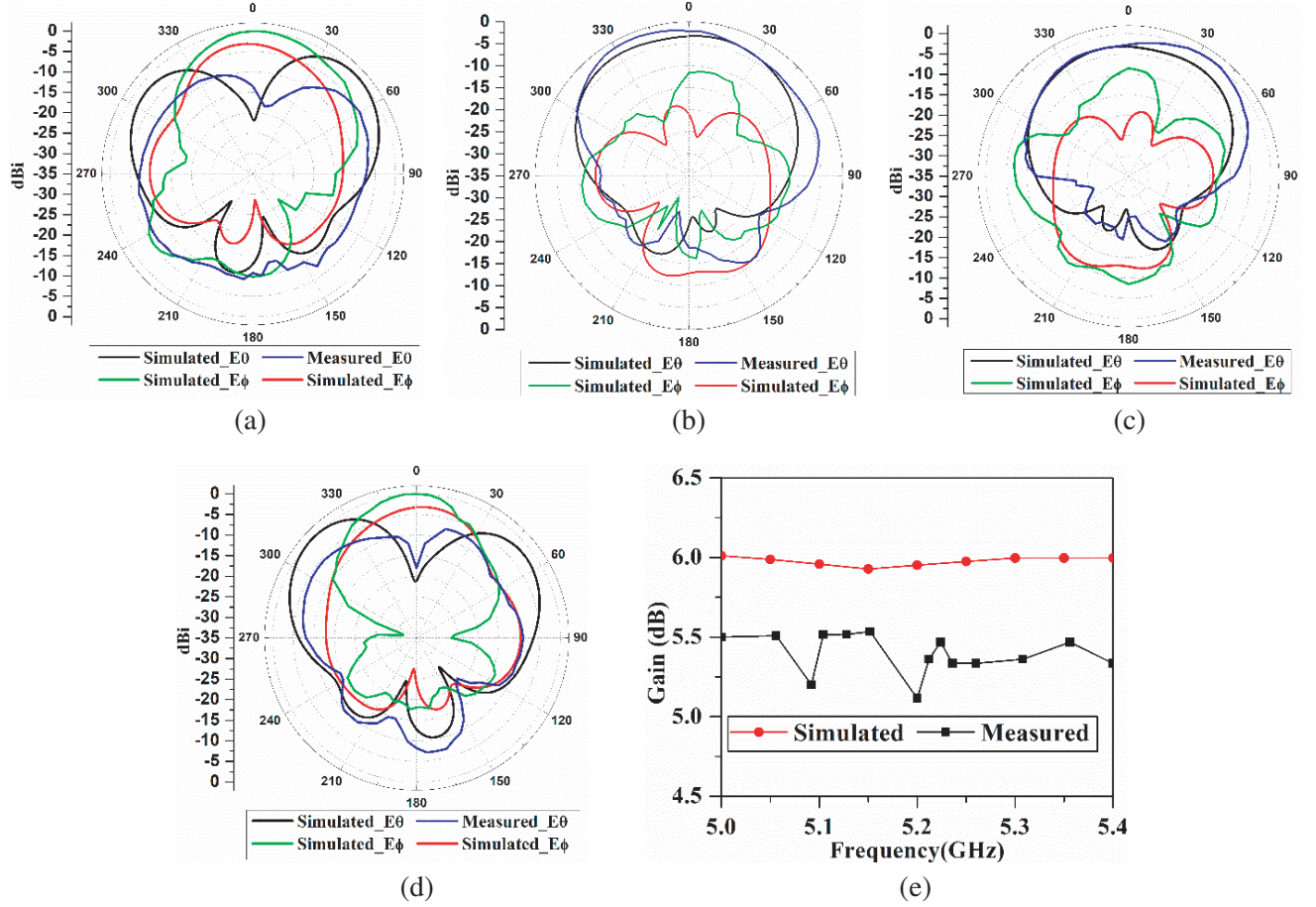


**Figure 5.** Normalized radiation pattern of proposed MIMO design, (a) in  $X$ - $Z$  plane while exciting Port 1, (b) in  $X$ - $Z$  plane while exciting Port 2, (c) in  $Y$ - $Z$  plane while exciting Port 1, (d) in  $Y$ - $Z$  plane while exciting Port 2, (e) gain.

The spatial correlation among elements (due to mutual coupling) of MIMO degrades the capacity, termed as the capacity loss (CL), and is calculated using Equation (5) for a high SNR case [19]. The measured minimum CL is close to 0.18 bits/Hz/sec at 5.1 GHz as depicted in Fig. 6(c)

$$CL = -\log_2 \det(\psi^r) \quad (5)$$

Here  $\psi^r$  is the  $4 \times 4$  correlation matrix with  $i, j = 1, 2, 3, 4$ .

$$\psi^r = \begin{bmatrix} \psi_{ii} & \dots & \psi_{ij} \\ \vdots & \ddots & \vdots \\ \psi_{ji} & \dots & \psi_{jj} \end{bmatrix}, \quad \psi_{ii} = 1 - (|S_{ii}|^2 + |S_{ij}|^2), \quad \psi_{ij} = -(S_{ii}^* S_{ij} + S_{ji}^* S_{jj})$$

The MEG (mean effective gain) quantifies the diversity performance of the MIMO system, where MEG is the ratio of mean received power to mean incident power, which includes the effects of antenna gain pattern and propagation characteristics (fading environment). For optimum performance, the ratio of  $MEG_i$  ( $i$ th antenna) to  $MEG_j$  ( $j$ th antenna) should approach unity or 0 dB as given in Equation (6), where MEG is expressed in Equation (7) [19]. Here ‘XPR’ is the cross-polarization ratio;  $P_\theta(\theta, \varphi)$  and  $P_\varphi(\theta, \varphi)$  are the angular density functions of received signals;  $G_{\theta i}(\theta, \varphi)$  and  $G_{\varphi i}(\theta, \varphi)$  are the theta and phi components of gain pattern for the  $i$ th antenna. For  $XPR = 0$  dB and uniform distribution for angular densities, the MEG is calculated using  $s$ -parameters given in Equation (8) [19].

A comparison of measured and simulated MEG and MEG ratios is shown in Fig. 6(d) and Fig. 6(e). It is observed that the MEGs of all ports are similar, and the MEG ratio approaches 0 dB (unity). The

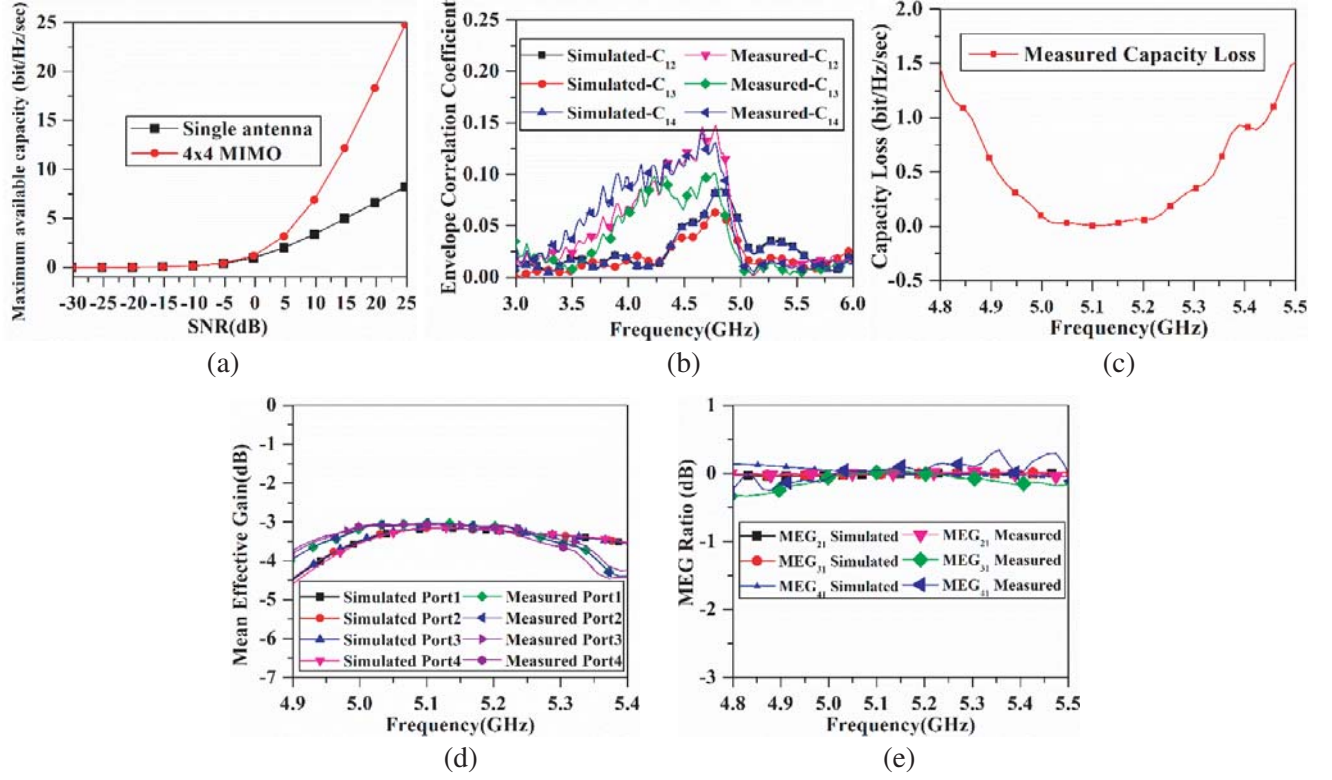


**Figure 6.** (a) Comparison of calculated values of maximum channel capacity of single element and proposed MIMO antenna. (b) Envelope correlation coefficient for signal received at portland transmitted from port 2 (C12), port 3 (C13), and port 4 (C14). (c) Measured capacity loss (CL), (d) MEG, (e) MEG<sub>ij</sub> ratio between *i*th port (1 port) and *j*th port.

slight difference between the measured and simulated values may be because of the manual fabrication tolerance and relatively high loss tangent of substrate material (FR4 substrate).

$$\frac{MEG_i}{MEG_j} \cong 1 \tag{6}$$

$$MEG_i = \oint \left[ \frac{XPR \cdot G_{\theta_i}(\theta, \phi) \cdot P_{\theta}(\theta, \phi) + G_{\phi_i}(\theta, \phi) \cdot P_{\phi}(\theta, \phi)}{1 + XPR} \right] d\theta d\phi \tag{7}$$

$$MEG_i = \frac{1 - \sum_{j=1}^N |S_{ij}|^2}{2} \tag{8}$$

DG (Diversity gain) is another important performance indicator of MIMO system, which is calculated using Equation (9) [15]. For the proposed MIMO design, calculated DG ranges from 9.9 to 9.98 dB in the band of operation as shown in Fig. 7. As the upper limit of DG is 10 dB, the proposed antenna exhibits a good MIMO performance.

$$DG_{ij} = 10 \times \sqrt{(1 - |ECC_{ij}|^2)} \tag{9}$$

A comparative study on the basis of MIMO performance and structural design are shown in Table 1 and Table 2, respectively. The proposed MIMO design has better isolation and high gain (6 dBi) n compared with four elements, dual-polarized, MIMO antennas [6, 7, 20]. Usually, multi-layer structures are used to attain higher gain, whereas compared with [4, 7], our proposed MIMO design has higher

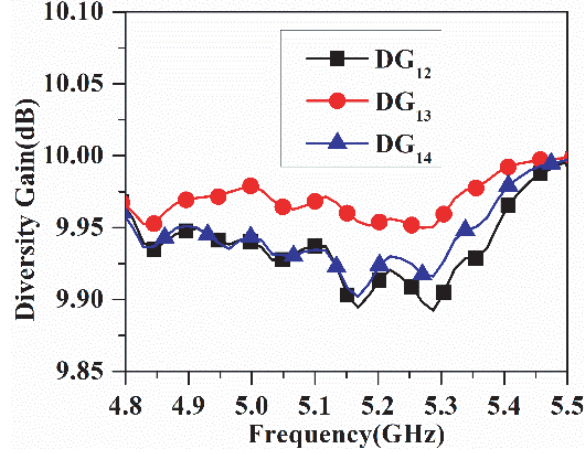


**Figure 7.** Calculated diversity gain  $DG_{ij}$  using measured  $ECC_{ij}$  between  $i$ th port (1 port) to  $j$ th port.

**Table 1.** Comparison of proposed MIMO design performance with the reported literature.

Ref. No.	Volumetric Size ( $\lambda^3$ )	Band-width (MHz)	Center Frequency (GHz)	Gain (dBi)	Isolation (dB)	Max-ECC (In-band)	Capacity Loss (bits /Hz/s)	No. of Elements
<b>This Work</b>	$1.1 \times 1.1 \times 0.027$	400	(5.2)	6	> 22	< 0.15	0.18	4
[4]	$0.84 \times 0.84 \times 0.33$	980	(2.2)	7	> 31	0.0042	-	2
[6]	$0.49 \times 0.49 \times 0.01$	75	(2.45)	3.4 to 4	> 22	< 0.4	-	4
[7]	$\pi \times 0.18 \times 0.11$	262	(0.829)	1.5	10 (adjacent) 15 (far)	0.075	-	4
[8]	$0.51 \times 0.44 \times 0.9$	700	(5.5)	2 to 3	> 16	0.05	-	2
[20]	$0.59 \times 0.59 \times 0.01$	400	(2.5)	3.67	> 17	0.04	< 0.6	4
[21]	$0.78 \times 0.93 \times 0.01$ , $1.3 \times 1.56 \times 0.026$ ,	Dual band 500, 2100	(5.85), (9.75)	3.5, 4.8	25	< 0.05	< 0.4	4
[22]	$0.79 \times 0.433 \times 0.037$	Ultra-Wide-Band, 7900	(7.05)	0.9 to 4	> 15 (3.1–5 GHz), > (5–11 GHz)	< 0.001	-	2
[23]	$0.19 \times 0.35 \times 0.004$ , $0.2 \times 0.37 \times 0.004$ , $0.4 \times 0.75 \times 0.009$ , $0.42 \times 0.79 \times 0.009$ , $0.54 \times 1 \times 0.012$ , $0.54 \times 1.02 \times 0.0126$ ,	Multi-band 9, 8, 23, 40, 34, 37	(0.826), (0.876), (1.743), (1.831), (2.339), (2.356)	2.26, 1.62, 3.42, 2.36, 2.84, 1.95	14 (0.850 GHz), 16.84 (1.8 GHz), –20.9 (2.3 GHz)	< 0.016	-	4

**Table 2.** Structural comparison of proposed MIMO design with the reported literature.

	Polarization /Diversity	Type of Ground	Number of Layers	Substrate Thickness (mm)
<b>This Work</b>	Dual/Pattern	Full ground	Single	FR4, ( $h = 1.6$ )
[4]	Dual/Pattern	Air filled electric cavity of height 39 mm	Multi	FR4, ( $h = 1.2$ (top))
[6]	Dual/Angle	CSRR	Single	FR4, ( $h = 1.6$ )
[7]	Single/NA	DGS	Multi	FR4, ( $h = 0.8$ ) + Polyethylene ( $h = 50$ )
[8]	Single/Pattern	DGS	Single	FR4, ( $h = 0.8$ )
[20]	Dual/Pattern	DGS with CSRR	Single	FR4, ( $h = 1.6$ )
[21]	Single/Pattern	DGS	Single	FR4, ( $h = 0.8$ )
[22]	Single/Pattern	DGS	Single	FR4, ( $h = 1.6$ )
[23]	Single/Frequency	Full ground	Single	FR4, ( $h = 1.6$ )

gain with respect to structure volume. Due to its simple structure and single layer, the proposed 4-element MIMO antenna can be easily mounted over any flat surface compared to all other reported designs [4, 6–8, 20–22]. The proposed MIMO design exhibits dual-polarization with high gain (6 dBi) compared with MIMO antennas with pattern diversity [21, 22] and frequency diversity [23].

## 5. CONCLUSION

A hammer-shaped element based, dual-polarized, high gain, and compact MIMO antenna has been demonstrated. In addition, a mathematical analysis has also been presented to analyze the radiating electric field of the hammer shaped element. The equivalent circuit of hammer shaped element has been developed successfully. The proposed MIMO antenna resonates at 5.2 GHz with approximate impedance bandwidth of 400 MHz. The proposed MIMO design has high isolation (22 dB), peak gain (5.5 dBi), and single layer geometry which make it suitable for handheld devices in WLAN band applications. The proposed MIMO design is suitable for different applications such as: applications requiring broader coverage area (by exciting all the ports simultaneously), beam scanning applications (by exciting one port at a time), and transceiver applications (by paring HP and VP as transmitter/receiver at a time).

## REFERENCES

1. Li, Q., et al., "MIMO techniques in WiMAX and LTE: A feature overview," *IEEE Communications Magazine*, Vol. 48, No. 5, 86–92, 2010.
2. Paul, T. and T. Ogunfunmi, "Wireless LAN comes of age: Understanding the IEEE 802.11n amendment," *IEEE Circuits and Systems Magazine*, Vol. 8, No. 1, 28–54, First Quarter 2008.
3. Chen, X., S. Zhang, and Q. Li, "A review of mutual coupling in MIMO systems," *IEEE Access*, Vol. 6, 24706–24719, 2018.
4. Lee, H. and B. Lee, "Compact broadband dual-polarized antenna for indoor MIMO wireless communication systems," *IEEE Transactions on Antennas and Propagation*, Vol. 64, No. 2, 766–770, 2016.

5. Zhu, J., S. Li, B. Feng, L. Deng, and S. Yin, "Compact dual-polarized UWB quasi-self-complementary MIMO/diversity antenna with band-rejection capability," *IEEE Antennas and Wireless Propagation Letters*, Vol. 15, 905–908, 2016.
6. Ramachandran, A., S. Valiyaveetil Pushpakaran, M. Pezholil, and V. Kesavath, "A four-port MIMO antenna using concentric square-ring patches loaded with CSRR for high isolation," *IEEE Antennas and Wireless Propagation Letters*, Vol. 15, 1196–1199, 2016.
7. Chen, Y. and C. Chang, "Design of a four-element multiple-input–multiple-output antenna for compact long-term evolution small-cell base stations," *IET Microwaves, Antennas & Propagation*, Vol. 10, No. 4, 385–392, 2016.
8. Hsu, C., L. Hwang, F. Chang, S. Wang, and C. Liu, "Investigation of a single-plate  $\pi$ -shaped multiple-input-multiple-output antenna with enhanced port isolation for 5 GHz band applications," *IET Microwaves, Antennas & Propagation*, Vol. 10, No. 5, 553–560, 2016.
9. Deng, J., L. Guo, and X. Liu, "An ultrawideband MIMO antenna with a high isolation," *IEEE Antennas and Wireless Propagation Letters*, Vol. 15, 182–185, 2016.
10. Qu, L., R. Zhang, and H. Kim, "Decoupling between ground radiation antennas with ground-coupled loop-type isolator for WLAN applications," *IET Microwaves, Antennas & Propagation*, Vol. 10, No. 5, 546–552, 2016.
11. Hussain, R. and M. S. Sharawi, "Planar meandered-F-shaped 4-element reconfigurable multiple-input-multiple-output antenna system with isolation enhancement for cognitive radio platforms," *IET Microwaves, Antennas & Propagation*, Vol. 10, No. 1, 45–52, 2016.
12. Gorai, A. and R. Ghatak, "Utilization of shorted fractal resonator topology for high isolation and ELC resonator for band suppression in compact MIMO UWB antenna," *AEU — International Journal of Electronics and Communications*, Vol. 113, 152978, 2020.
13. Bakariya, P. S., S. Dwari, and M. Sarkar, "Triple band notch UWB printed monopole antenna with enhanced bandwidth," *AEU — International Journal of Electronics and Communications*, Vol. 69, No. 1, Art. No. 1, 2015.
14. Atallah, H. A., A. B. Abdel-Rahman, K. Yoshitomi, and R. K. Pokharel, "CPW-fed UWB antenna with sharp and high rejection multiple notched bands using stub loaded meander line resonator," *AEU — International Journal of Electronics and Communications*, Vol. 83, 22–31, 2018.
15. Deng, C., Z. Feng, and S. V. Hum, "MIMO Mobile handset antenna merging characteristic modes for increased bandwidth," *IEEE Transactions on Antennas and Propagation*, Vol. 64, No. 7, Art. No. 7, 2016.
16. Balanis, C. A., *Antenna Theory: Analysis and Design*, John Wiley & Sons, In, 2005.
17. Valagiannopoulos, C. A. and N. L. Tsitsas, "On the resonance and radiation characteristics of multi-layered spherical microstrip antennas," *Electromagnetics*, Vol. 28, No. 4, 243–264, May 2008.
18. Valagiannopoulos, C. A., "Semi-analytic solution to a cylindrical microstrip with inhomogeneous substrate," *Electromagnetics*, Vol. 27, No. 8, 527–544, Nov. 2007.
19. Sharma, V., A. Goel, M. D. Upadhyay, and A. V. Singh, "A Pi-shaped slot antenna for 5.2 GHz WLANMIMO application," *IETE J. Res.*, 1–13, Jan. 2021.
20. Yussuf, A. A. and S. Paker, "Design of a compact quad-radiating element MIMO antenna for LTE/Wi-Fi application," *AEU — International Journal of Electronics and Communications*, Vol. 111, 152893, 2019.
21. Yalavarthi, U. D., R. T. Koosam, M. N. S. D. Venna, and B. S. Thota, "Four element square patch MIMO antenna for DSRC, WLAN, and X-band applications," *Progress In Electromagnetics Research M*, Vol. 100, 175–186, 2021.
22. Khan, M. K., Q. Feng, and Z. Zheng, "Experimental investigation and design of UWB MIMO antenna with enhanced isolation," *Progress In Electromagnetics Research C*, Vol. 107, 287–297, 2021.
23. Goud, J. R., N. V. K. Rao, and A. M. Prasad, "Design of triple band U-slot MIMO antenna for simultaneous uplink and downlink communications," *Progress In Electromagnetics Research C*, Vol. 106, 271–283, 2020.